Target design for high fusion yield with the double Z-pinch-driven hohlraum[a)]

R. A. Vesey,[b)] M. C. Herrmann, R. W. Lemke, M. P. Desjarlais, M. E. Cuneo, W. A. Stygar, G. R. Bennett, R. B. Campbell, P. J. Christenson, T. A. Mehlhorn, J. L. Porter, and S. A. Slutz
Sandia National Laboratories, P.O. Box 5800, Albuquerque, New Mexico 87185-1186

(Received 29 October 2006; accepted 11 January 2007; published online 22 March 2007)

A key demonstration on the path to inertial fusion energy is the achievement of high fusion yield (hundreds of MJ) and high target gain. Toward this goal, an indirect-drive high-yield inertial confinement fusion (ICF) target involving two Z-pinch x-ray sources heating a central secondary hohlraum is described by Hammer *et al.* [Phys. Plasmas **6**, 2129 (1999)]. In subsequent research at Sandia National Laboratories, theoretical/computational models have been developed and an extensive series of validation experiments have been performed to study hohlraum energetics, capsule coupling, and capsule implosion symmetry for this system. These models have been used to design a high-yield Z-pinch-driven ICF target that incorporates the latest experience in capsule design, hohlraum symmetry control, and x-ray production by Z pinches. An x-ray energy output of 9 MJ per pinch, suitably pulse-shaped, is sufficient for this concept to drive 0.3–0.5 GJ capsules. For the first time, integrated two-dimensional (2D) hohlraum/capsule radiation-hydrodynamics simulations have demonstrated adequate hohlraum coupling, time-dependent radiation symmetry control, and the successful implosion, ignition, and burn of a high-yield capsule in the double Z-pinch hohlraum. An important new feature of this target design is mode-selective symmetry control: the use of burn-through shields offset from the capsule that selectively tune certain low-order asymmetry modes (P_2, P_4) without significantly perturbing higher-order modes and without a significant energy penalty. This paper will describe the capsule and hohlraum design that have produced 0.4–0.5 GJ yields in 2D simulations, provide a preliminary estimate of the Z-pinch load and accelerator requirements necessary to drive the system, and suggest future directions for target design work. © *2007 American Institute of Physics*. [DOI: 10.1063/1.2472364]

I. INTRODUCTION

Z pinches driven by fast pulsed-power (~100 ns current pulses) are very efficient sources of soft x rays,[1] and their potential for indirect-drive inertial confinement fusion (ICF) is currently being explored in a variety of approaches. One approach is the high-yield concept proposed by Hammer *et al.*,[2] which uses a Z-pinch-driven primary hohlraum at each end of a central coaxial secondary hohlraum containing the ICF capsule. Figure 1 illustrates the features of the hohlraum geometry relevant for this hohlraum concept. This vacuum hohlraum-based concept has been developed as an experimental platform on the Z accelerator[3] at Sandia National Laboratories. This platform has provided high quality data to validate the numerical simulations of this concept. Experiments conducted over the past several years have quantified the Z-pinch power, primary hohlraum radiation temperatures, and primary-secondary hohlraum coupling efficiency for configurations relevant to this concept.[4–7] Viewfactor and radiation-hydrodynamics models have been used to design hohlraums that tune the capsule radiation symmetry for near-term experiments.[8,9] An advanced double Z-pinch wire-array load driven by a single power feed has been developed that provides upper and lower pinch x-ray power histories that are balanced such that measurements of upper and lower primary hohlraum wall emission temperatures agree within instrumental error bars.[10] For symmetry diagnosis, the Z-Beamlet Laser[11] is being used to create high-energy x rays for point projection backlighting[12] and bent-crystal imaging[13] of capsule implosions in double Z-pinch hohlraums. Backlit capsule images on Z have enabled measurements of implosion trajectories as well as in-flight distortions at the percent level[12] for the first time in Z-pinch-driven hohlraums, and a hohlraum length scan demonstrated that pole-to-equator radiation asymmetry can be predictably zeroed as a function of secondary hohlraum geometry.[14,15] Several years of validation experiments[16,17] provide confidence in the modeling capability that will now be applied to updating the high-yield target design. A review of eight years of experiments and simulations on the double Z-pinch platform has been published recently.[18]

The initial scoping study of the double Z-pinch hohlraum by Hammer *et al.*[2] identified many key physics issues, quantified the energetics of such a system, and provided the starting point for the present study. The previous study used a circuit model of the Z accelerator, with the open-circuit voltage scaled up, to drive two-dimensional (2D) simulations of Z-pinch performance. At peak currents of 63 MA, a multishell Z pinch composed of low-Z materials (lithium deuteride) was calculated to provide a useful x-ray pulse shape

[a)]Paper BI2 2, Bull. Am. Phys. Soc. **51**, 23 (2006).
[b)]Invited speaker.

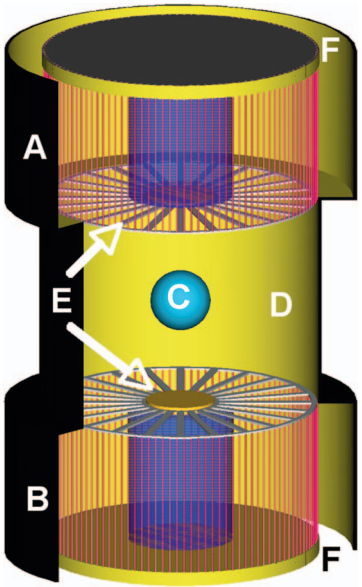

FIG. 1. (Color) Double Z-pinch hohlraum concept. (A) and (B) top and bottom primary hohlraums, containing notional wire array Z pinch with internal pulse-shaping targets. (C) High-yield capsule, (D) secondary hohlraum containing the capsule, (E) on-axis permanent shine shield and radial spoke electrode structures, and (F) upper and lower electrical power feeds.

with peak powers of order 1000 TW and total x-ray energy outputs of 8–10 MJ per pinch (depending on assumed perturbation levels). Using the calculated Z-pinch output as input to 2D hohlraum calculations, shaped capsule drive temperature pulses with peak temperatures of 210 eV were obtained. The time-dependent behavior of the radial spoke arrays that separate the primary and secondary hohlraums was calculated to provide adequate hohlraum coupling while confining the magnetic field to the primary hohlraum, and the sensitivity of the hohlraum energetics to the effective spoke transmission was quantified. Finally, a high-yield capsule was found to be compatible with the calculated drive pulse; the capsule absorbs 1 MJ of x rays with a fusion yield of 400 MJ. This scoping study highlighted the crucial issues for this high-yield target concept that have been the objects of subsequent experimental study on Z and that are the objects of the present design study: Z-pinch x-ray pulse shaping, hohlraum energetics and coupling, radiation symmetry control, and capsule robustness. The main new result presented in this paper is the development of a complete strategy for radiation symmetry control that allows for robust capsule ignition and burn in 2D hohlraum simulations, a necessary achievement for any modern ICF target design.

II. HIGH-YIELD CAPSULE DESIGN

A. Characteristics and one-dimensional performance

The original double Z-pinch hohlraum reference[2] described a 400 MJ yield capsule with a beryllium ablator to be driven by a pulse with a peak radiation temperature ~210 eV. The capsule chosen for the present design is similar to the earlier capsule. The main fuel is a cryogenic deuterium-tritium (DT) layer deposited on the inside of the spherical ablator shell. The ablator is composed of beryllium,

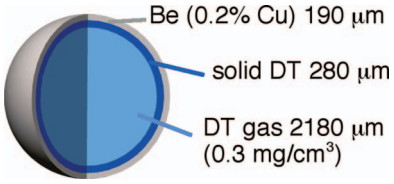

FIG. 2. (Color) High-yield capsule schematic.

doped uniformly with 0.2 at. % of copper to mitigate preheat of the DT fuel by the higher energy photons in the tail of a 220 eV Planckian distribution. Figure 2 shows schematically the baseline capsule chosen for the present study, while Fig. 3 shows the time-dependent radiation temperature $T_r(t)$ used in simulations to design the capsule. The model temperature history shown contains three distinct features: a "foot" pulse of 95 eV, a "shoulder" step of 130 eV, and a "peak" temperature pulse of 223 eV. The characteristics and performance of the baseline capsule in one-dimensional (1D) LASNEX[19] simulations are summarized in Table I. For comparison, also shown in Table I are the corresponding values for a graded-dopant Be-Cu capsule designed for a peak 300 eV effective temperature drive for the upcoming National Ignition Facility (NIF) laser indirect-drive ignition campaign.[20] The high-yield capsule is 2.65 times larger in radius than the NIF capsule, with 30 times more DT fuel. With an absorbed energy of 1.21 MJ, the high-yield capsule does not require as high an implosion velocity as the NIF capsule, so the peak ablation pressure is ~60 Mbar compared to the 160 Mbar for the NIF capsule. As a result, the high-yield capsule can be driven with a simpler pulse shape than the four distinct temperature steps required for the NIF capsule.[2] The hot-spot convergence ratio, and the fuel kinetic energy margin (the fraction of the peak fuel implosion kinetic energy remaining at ignition time) are comparable for the two capsules.

B. Pulse shape tolerance

Capsule-only radiation-hydrodynamics simulations are used to evaluate several possible capsule failure modes, such as pulse shape sensitivity, unstable growth of initial capsule perturbations, and hohlraum radiation asymmetry. The first of these, pulse shape sensitivity, is essentially a one-

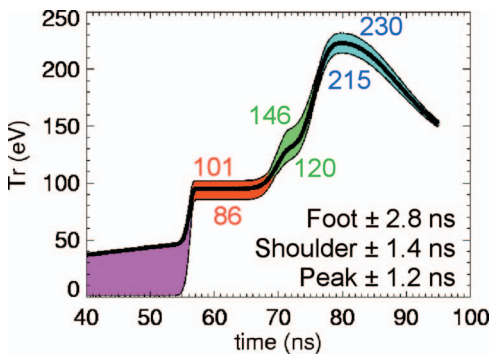

FIG. 3. (Color) Temperature history assumed for capsule design, with tolerable variations.

TABLE I. Characteristics and performance parameters for the baseline 520 MJ double Z-pinch capsule.

Capsule	NIF layered Be 300 eV	Double Z-pinch 220 eV
Ablator outer radius (mm)	1.1	2.65
Ablator thickness (μm)	160	190
DT fuel thickness (μm)	80	280
Absorbed energy (MJ)	0.14	1.21
Yield (MJ)	13	520
Peak total ρr (g/cm^2)	1.9	3.1
Fuel mass-weighted implosion velocity (cm/μs)	36.4	26.0
Minimum fuel adiabat α_{if}	0.93	0.74
Fuel mass fraction at $>1.5\ \alpha_{if}$	0.06	0.06
Drive pressure (MB)	160	60
In-flight aspect ratio	19	35
Fuel KE remaining at ignition	33%	29%
Hot-spot convergence ratio	36	34

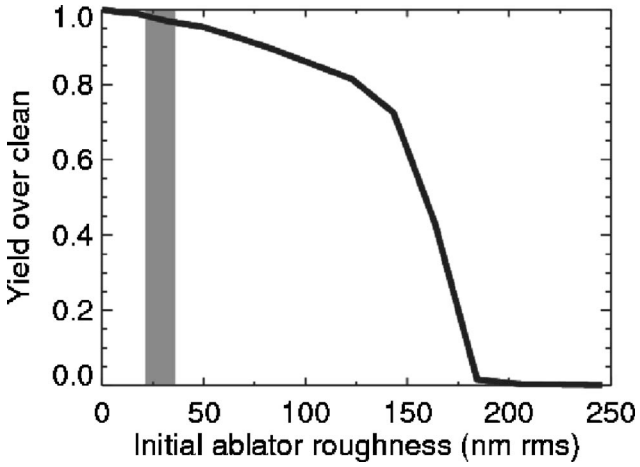

FIG. 4. Capsule yield vs rms surface roughness for multimode simulations. (The vertical band is the NIF specification for outer Be surface roughness for modes 12 and greater.)

dimensional failure mode. The values of DT fuel in-flight minimum adiabat α_{if}, and the mass fraction of the DT fuel on a high adiabat ($>1.5\alpha_{if}$) shown in Table I, indicate that the model $T_r(t)$ pulse maintains the fuel at low entropy during the implosion, resulting in high peak fuel density and areal density, which provide efficient fusion burn. [The fuel adiabat α is defined as $P/(2.18\rho^{5/3})$ where P is the pressure in Mbar and ρ is the density in g/cc.[21]] As Fig. 3 illustrates, the baseline capsule can tolerate relatively large deviations away from the model temperature history and still give nearly full yield, corresponding to factors of 1.9, 2.2, and 1.3 full ranges in the incident radiation flux in the foot, shoulder, and peak pulse, respectively. The radiation prior to the foot is generated during the pinch implosion by ohmic heating of the Z pinch and is not necessary for good capsule performance. In fact, this run-in radiation may lead to early time imprinting of radiation asymmetries, growth of surface perturbations without significant ablative stabilization, and imprinting of beryllium microstructure variations prior to the multi-Mbar foot shock passing through the ablator. If necessary, tamping foams at the secondary hohlraum entrance can be designed to absorb essentially all of the run-in radiation to prevent it from affecting the capsule implosion. Note that the T_r variations shown in Fig. 3 are single-feature variations; for example, the foot temperature can vary within the 86 to 101 eV range as long as the remainder of the pulse follows the baseline $T_r(t)$ history. Likewise, the timing of the foot, shoulder, and peak pulses can vary by ±2.8, 1.4, and 1.2 ns, respectively, without degrading the capsule yield. The maximum and minimum allowable timing variations are determined by the need to prevent successive shocks from coalescing inside the DT ice layer and to limit the amount of fuel rarefaction that occurs after a shock breaks out from the inner surface of the DT ice.[21]

C. Capsule surface perturbation tolerance

Initial perturbations on surfaces and material interfaces within the capsule will grow during the capsule acceleration and deceleration due to the Rayleigh-Taylor (RT) instability. Excessive growth of perturbations will cause degradation of the fusion burn and, with large enough perturbations, failure of the capsule to ignite by degrading the final compression phase which forms the hot spot. Two-dimensional (2D) LASNEX radiation-hydrodynamics simulations model the effects of RT instability by studying the growth from a full spectrum of modes typical of fabricated ablator shells.[22–25] The preliminary multimode calculations described here use the same methodology used previously for ignition capsules.[22,23,25] A 15° wedge of the capsule near the equator is modeled which allows for one-half wavelength of mode 12, while the angular resolution for practical calculations is chosen to resolve up to mode 160. An inline equation of state[26] is used, and another key feature is the collapsed-group opacity scheme of Marinak *et al.*,[27] which enables accurate calculations with relatively few photon energy groups for these problems. Figure 4 shows the calculated capsule yield (relative to the unperturbed yield) as a function of rms surface roughness in modes up to 160, assuming the NIF standard mode spectrum[22,24,28] describes the initial surface perturbation. As Fig. 4 shows, high mode surface perturbations lead to a fairly gradual decrease of the capsule yield as a function of initial perturbation, due to higher frequency variations in the fuel ρr that degrade the burn efficiency. Thus, while the high-yield capsule still forms a self-heating hot spot even at 200 nm roughness, the quality of the burn propagation and thus the yield are drastically reduced compared to the unperturbed case. For comparison with the high-yield target, a recently published 0.9% Cu-doped Be capsule with radius 1.11 mm, with a peak drive temperature of 300 eV, absorbed energy of ~150 kJ, and yield of 20 MJ, gives 50% of full yield at an ablator roughness of ~220 nm.[29] Even more encouraging from the optimization point of view is that a variation on the 300 eV capsule mentioned above, using radially varying levels of Cu dopant, was calculated to tolerate ~600 nm rms surface roughness before failure.[29] Present-day target fabrication technology for Cu-doped Be shells (albeit at 1 mm radius), with sputter coating followed by polishing, is capable of producing Be surface finishes near the NIF specifi-

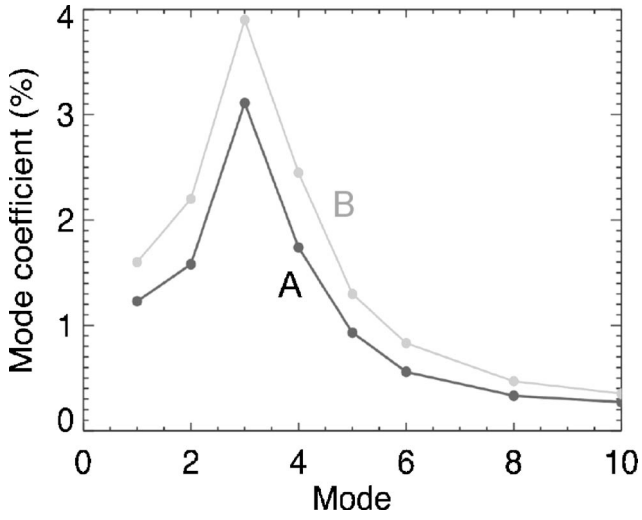

FIG. 5. Capsule yield vs constant-in-time radiation asymmetry by mode. (A) Baseline 520 MJ capsule with 280 μm fuel layer. (B) Alternate 410 MJ capsule with 230 μm fuel layer.

cation of ~36 nm for modes 12 and greater,[30] a factor of 4 below the point at which the high-yield capsule fails.

D. Radiation asymmetry tolerance

A perfectly spherical capsule will undergo an aspherical implosion if the radiation field driving it is spatially nonuniform. Although a hohlraum naturally smooths the x-ray distribution within it, ignition capsules require a very high degree of x-ray symmetry in order to remain nearly spherical to radial convergence ratios of 30 or greater. A series of capsule-only 2D LASNEX simulations identify, for each mode, the Legendre mode coefficient of the flux asymmetry (constant in time over the entire drive pulse) that causes the capsule fusion yield to be degraded by 50% compared to the uniform-drive case. Unlike the short-wavelength perturbations described in the previous section, long-wavelength radiation asymmetry does not significantly degrade the burn propagation of an igniting capsule, but rather at high enough amplitude leads to a failure to ignite. Thus, a plot of capsule yield versus increasing mode amplitude generally exhibits a flat plateau and then a rapid drop to non-ignition (the "ignition cliff"). The mode amplitudes at which the ignition cliff occurs are plotted in Fig. 5, for the baseline 520 MJ capsule and for a 410 MJ capsule that has a thinner fuel layer and correspondingly higher peak implosion velocity of 28.6 cm/μs (10% higher velocity than for the baseline capsule). Here we have included calculations for odd Legendre modes P_1, P_3, and P_5, as well as even modes P_2 through P_{10}.

In general, the capsule tolerates less asymmetry as the mode number increases, although an interesting mode inversion effect occurs near mode 3 for this capsule and drive pulse. This effect was also noted in NIF capsule simulations by Pollaine *et al.*,[31] although modes P_1, P_3, and P_5 were not included in that study. For modes P_1 and P_2, the shape of the compressed DT fuel and hot spot preserves the phase of the applied asymmetry mode, in the sense that a positive P_1 asymmetry with a higher applied flux at the bottom pole of the capsule results in a higher density feature and a smaller local hot-spot radius at the bottom pole. For modes 4 and higher, the compressed fuel shows higher density features and a smaller local hot-spot radius at polar angles where the flux was *lowest*; in this sense the applied mode has inverted during the implosion. (As the applied asymmetry is increased, these features become jets which cause the capsule to fail.) For P_3, although the shape of the compressed fuel clearly reflects the applied P_3 flux asymmetry, significant polar variations in the fuel areal density at ignition time appear with higher flux asymmetry coefficients than for the other modes. With increasing P_3, the capsule ignition is delayed and is eventually prevented at high mode amplitudes by an on-axis jet. (Although it is remarkable that this capsule is very insensitive to P_3 in the calculations, this is not a critical feature of the high-yield target design.)

Although this capsule has not been optimized for robustness, its relative insensitivity to pulse shape as well as the calculated tolerances for radiation asymmetry and capsule surface finish indicate that it is a good candidate to include in the more integrated hohlraum+capsule simulations described below. Figure 5 showed one possible variation that increases the capsule robustness to asymmetry: a thinner fuel layer and slightly shorter foot pulse that led to a 10% higher fuel implosion velocity, as suggested in Ref. 31. The effect of higher implosion velocity on the surface finish tolerance will be evaluated. Another variation mentioned earlier is the use of radially-graded Cu dopant in the Be ablator,[22,29] which may improve the robustness to surface perturbations by simultaneously increasing the ablation velocity and gradient scale length while decreasing the Atwood number at the fuel-ablator interface.

III. INTEGRATED HOHLRAUM AND CAPSULE SIMULATIONS

A. 2D LASNEX simulation setup

The most complete physical model currently available for the double Z-pinch hohlraum is provided by the LASNEX 2D radiation magnetohydrodynamics (RMHD) code.[19] The models presented here have built directly on the earlier work by Hammer and Tabak.[2] Figure 6 shows the initial simulation setup for the standard two-sided feed configuration of the double Z-pinch hohlraum in which the two Z-pinches are driven by a single accelerator via separate magnetically-insulated transmission lines (MITLs) at the top and bottom. Each primary hohlraum is 1.25 cm in radius, 1.0 cm in length, with an assumed Z-pinch load initial outer radius of 1.05 cm. The aperture at the entrance to the secondary hohlraum has an inner radius of 0.3 cm defined by the on-axis shine shield and an outer radius of 1.0 cm defined by the secondary hohlraum radius. LASNEX simulations of this configuration include hohlraum walls composed of gold-gadolinium (1:1 atomic mix) to increase x-ray opacity and reduce energy losses to the walls.[2,32] Currently, the Z-pinch source is included as a moving cylindrical x-ray source with a prescribed trajectory $r(t)$, prescribed x-ray power history $P_{\mathrm{rad}}(t)$, and with a prescribed associated current $I(t)$. The prescribed $r(t)$, $P_{\mathrm{rad}}(t)$, and $I(t)$ are inputs to the hohlraum

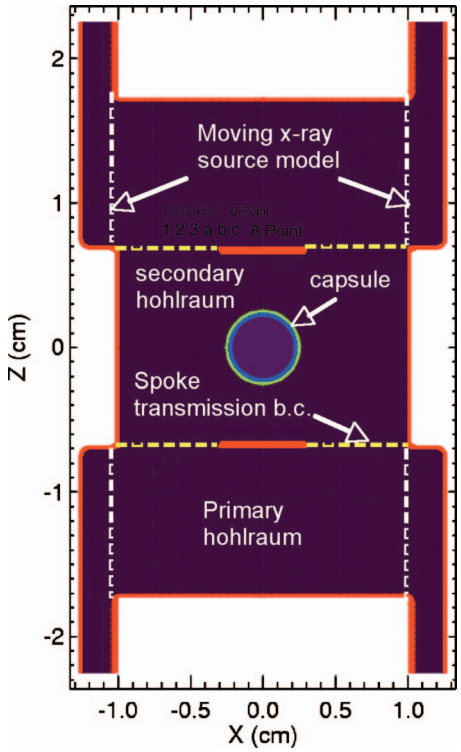

FIG. 6. (Color) LASNEX setup for 2D simulations.

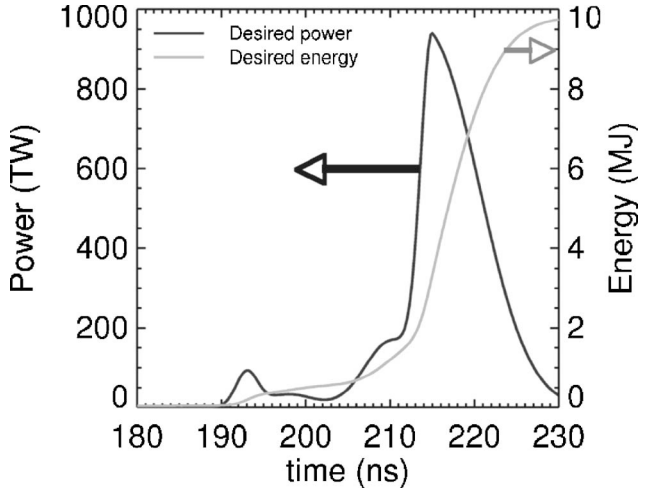

FIG. 7. Ideal Z-pinch x-ray power history and the running integral of the radiated energy for required three-step pulse.

simulation and may be idealized histories, calculated outputs from separate two- and three-dimensional (3D) Z-pinch simulations, or based on experimental measurements.

The main physics included in the 2D LASNEX hohlraum simulations is multigroup radiation transport, hohlraum wall and symmetry shield RHD, capsule implosion RHD, and capsule ignition and burn physics. The main goals of such simulations are to calculate the transport of x-rays from the Z-pinch source to the capsule, to calculate the asymmetry of the radiation incident on the capsule, and to calculate the capsule implosion, ignition, and burn. As mentioned, the Z-pinch implosion is not self-consistently included; however, the time-dependent Z-pinch current is driven through the anode and cathode walls of the primary hohlraums to calculate magnetic tamping of the hohlraum wall plasma. The magnetic field is assumed to be confined within the primary hohlraums due to the presence of the spoke electrodes. As is common in 2D LASNEX simulations of hohlraums,[33] neither 3D effects nor high-mode RT instability of the capsules is included. Except when these simulations are used to calculate the effects of top-bottom pinch power imbalance or mistiming, half of the system is modeled and a perfect symmetry boundary condition is applied at the midplane (cutting through the equator of the capsule).

The radial spoke arrays located at each entrance to the secondary hohlraum are not self-consistently included; a time-dependent x-ray transmission boundary condition is applied based on separate calculations of spoke dynamics.[2] These separate 2D RMHD simulations model a cross section of a single spoke with periodic boundary conditions to account for neighboring spokes in the array; time-dependent external radiation temperature sources simulate the hohlraum environment and a magnetic field source applies the effects of a prescribed time-dependent current carried by the spokes. Not included in these spoke simulations is any effect of the imploding Z-pinch plasma, secondary hohlraum wall, or on-axis shine shield. Nonetheless, experiments at the Z facility have validated most aspects of the calculated performance of radial spoke arrays: (1) Time-gated x-ray images clearly demonstrate that the spokes remain intact throughout the power pulse,[6,34] (2) measurements of energy flow from the primary to secondary hohlraum is consistent with an average spoke transmission of 71% ±7% at peak power in agreement with the calculated value of 75%,[6,7] and (3) the measured Z-pinch power pulse for loads with and without spokes agree within the error bars.[6] The inclusion of an x-ray transmission boundary condition has proven useful in previous 2D LASNEX hohlraum simulations to successfully explain hohlraum coupling[6,17] as well as capsule symmetry control.[15,18] Future work with emerging 3D RMHD simulation tools will be required to study the hydrodynamic interactions with nearby hohlraum structures as well as to model the 3D problem of a Z-pinch imploding along a radial spoke array electrode, to more accurately model the physics of the secondary entrance region.

The desired Z-pinch x-ray power history required to produce the capsule temperature drive shown in Fig. 3 is calculated using 2D LASNEX hohlraum simulations. Iteratively, the prescribed pinch power history is adjusted until the calculated $T_r(t)$ at the capsule location matches the desired $T_r(t)$. Figure 7 shows the ideal Z-pinch x-ray power history and the running integral of the radiated energy. As noted in Table I, the high-yield capsule has a lower required peak ablation pressure than the comparison NIF capsule; the desired pulse shape requires only three distinct temperature steps. Nonetheless, the pulse shaping keeps the fuel on a low adiabat as noted earlier. For each 1 cm long pinch, the radiated energy required is 0.50, 1.37, and 9.0 MJ at times of −15, −4, and +9 ns relative to the time of peak power. Producing this ideal Z-pinch power pulse then becomes the goal of the Z-pinch load design simulations (discussed later). Qualitatively, the

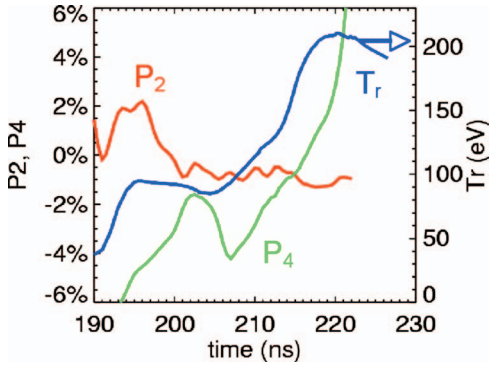

FIG. 8. (Color) Time-dependent P_2 and P_4 Legendre modes of the ablation pressure along with the spatially averaged time-dependent radiation temperature sampled at radii of 1.3–1.6 times the initial capsule radius, for the hohlraum configuration of Fig. 7.

ideal power pulse is similar to the results shown by Hammer[2] in terms of peak-to-foot power contrast and timing. Because it satisfies the energy requirements of the capsule, this ideal pulse will be used as input to the hohlraum+capsule simulations to study time-dependent symmetry control.

B. Radiation symmetry control strategy

Without additional symmetry control structures in the double Z-pinch hohlraum shown in Fig. 6, the radiation incident on the capsule is quite symmetric, owing to the large ratio of the wall surface area to the capsule surface area. As has been discussed previously,[7] about 70% of the radiation entering the secondary hohlraum is due to primary hohlraum wall re-emission, one level of spectral and spatial smoothing. Of the radiation incident on the capsule, 75%–80% is due to secondary hohlraum wall re-emission and 20%–25% is due to primary hohlraum wall emission.[15] (Because of the on-axis shine shield, ideally none of the Z-pinch radiation at stagnation directly illuminates the capsule.) The combination of re-emission smoothing within the hohlraum and geometric averaging at the capsule[35] results in a fairly symmetric x-ray flux distribution on the capsule. LASNEX simulations of the hohlraum+capsule configuration of Fig. 6 show low time-averaged radiation asymmetry, as evidenced by the polar asymmetry of the ablation pressure in the capsule. Figure 8 plots the time-dependent P_2 and P_4 Legendre modes of the ablation pressure along with the spatially averaged time-dependent radiation temperature sampled at radii of 1.3–1.6 times the initial capsule radius. The time period from 190 to 210 ns on this plot will be referred to as the "foot/shoulder" phase, and 210 to 220 ns will be referred to as the "peak."

It is clear from Fig. 8 that P_4 is significant and negative during the foot/shoulder; the time-averaged P_4 is −3.3% during this phase, while the time-averaged P_2, P_6, and P_8 are all less than 0.2%. The negative P_4 corresponds to a surplus of flux from regions of the hohlraum sky at ~45° relative to the z axis; the sources are the higher temperature primary hohlraum walls and the axial temperature gradient along the secondary hohlraum wall. During the main pulse, the secondary hohlraum heats up and reduces the temperature gradients, while the capsule begins to implode and increases the case:capsule ratio, and both effects move the P_4 asymmetry in the positive direction. Control of the P_2 asymmetry mode is accomplished by the choice of secondary hohlraum length (14.5 mm in this case). The effect on P_2 of varying the secondary hohlraum length has been quantitatively verified in double-pinch hohlraum experiments at the Z facility.[14,15,18] The −3.3% P_4 is large enough by itself to spoil the capsule implosion; the resulting calculated fusion yield is 40 kJ and the compressed DT fuel is strongly disrupted with a clear P_4 shape (with mode phase inverted as mentioned in Sec. II C). This level of P_4 is also consistent with x-ray backlit capsule measurements under foot-like conditions for double Z-pinch hohlraums on the Z facility.[18,36] Previous simulation results for Z conditions suggested that the negative P_4 could be reduced by (a) using a smaller on-axis shine shield, or (b) using larger radius primary hohlraums. Experiments with a smaller on-axis shine shield of 2.4 mm diameter indicated a possible reduction in the magnitude of P_4, but a large increase in positive P_2 (pole-hot) due to direct shine from the stagnated Z pinch.[37] The effect on P_4 of larger radius primary hohlraums (for fixed secondary hohlraum geometry) has not been tested experimentally; the possible beneficial effect on P_4 would have to be weighed against the potentially large penalty on hohlraum efficiency. Thus, a new design solution is desired for the high-yield concept, to control P_4 while preserving the low levels of P_6, P_8, and higher modes that are obtained due to geometric averaging in the hohlraum.

Shields in various forms have been previously proposed and used for symmetry control in hohlraum designs.[38] The on-axis shine shield already present in the double Z-pinch hohlraum eliminates a gross pole-hot flux that would be seen by the capsule due to Z-pinch stagnation radiation. The symmetry shield design strategy described below is akin to the capsule shimming approach,[39] but offsets the symmetry control structures from the capsule surface to avoid potential hydrodynamic coupling of the shield to the capsule. Consider a set of purely absorbing, non-expanding shields, each defined as a section of a sphere with material occupying a specific polar angle range. The example of a ring shield occupying θ_1 to θ_2 is shown in Fig. 9. Identical ring shields are located above and below the equator of the capsule, to avoid introducing odd Legendre mode components (P_1, etc.). (Of course, one could also compensate for a known P_1 asymmetry by choosing different shields above and below the capsule equator.) A detailed discussion of symmetry control with mode-specific shields will appear in a future publication. For the purpose of this discussion, we begin by approximating the contribution of a ring shield to Legendre mode n of the capsule-incident flux as being proportional to the following source-weighted and absorption-weighted integral:

$$a_n \propto \int_{-1}^{1} w(x)S(x)P_n(x)dx, \tag{1}$$

where $x=\cos(\theta)$, $S(x)$ is the relative source intensity distribution, and $P_n(x)$ is the Legendre polynomial of order n. In general, $w(x)$ is an absorption coefficient due to the shield,

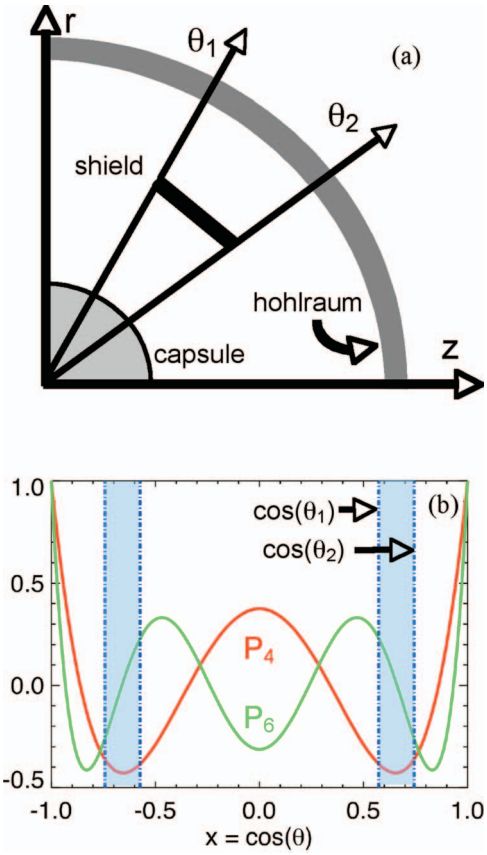

FIG. 9. (Color) (a) Shield ring schematic and (b) mapping onto cos(θ) space.

but for this paper, $w(x)$ is assumed to be a step function, equal to unity inside the shield angular range and zero elsewhere. For the specific case shown in Fig. 9(a), $w(x)=1.0$ for $\theta_1<\theta<\theta_2$, $w(x)=1.0$ for $(\pi-\theta_2)<\theta<(\pi-\theta_1)$, and $w(x)=0.0$ elsewhere.

The design problem is to correct P_4 without perturbing higher-order modes; in this case we seek to have zero effect on P_6. Figure 9(b) maps one possible shield solution onto cos(θ) space, with the P_4 and P_6 polynomials overlaid. It is clear from the figure that the example shown will have an effect on P_4 (the integral of P_4 over the shield extent will be nonzero), while it is conceivable that the same shield would have a small effect on P_6 (the integral of P_6 over the shield extent is near zero). This observation suggests the following approach. For each value of $x_1=\cos(\theta_1)$, the following polynomial equation was solved:

$$\int_{x_1}^{x_2} P_6(x)dx = 0. \tag{2}$$

Trivial and complex solutions of Eq. (2) were discarded, resulting in a set of shield solutions that have zero P_6 content, and varying P_4 content. These shield solutions were tested in viewfactor simulations, quantitatively confirming the postulate of expression (1). Shield rings from this family of solutions were then included in a series of 2D LASNEX hohlraum simulations, which included the radiation-driven ablation, expansion, and burn-through of the shields. As was shown in Fig. 8, the P_4 asymmetry is largest during the foot/shoulder phase, so the shields were designed to burn through and become optically thin near the end of this phase. Figure 10 plots the LASNEX simulation results for the foot/shoulder time-averaged values of P_4 through P_8 as a function of the shield angular extent ($\theta_1-\theta_2$, where each choice is a "zero P_6" solution). The shields clearly provide control of P_4 with relatively small perturbation of P_6 and P_8. The P_2 asymmetry trends toward negative coefficients (equator hot) as a function of increasing shield size, but this effect can be independently compensated with hohlraum geometry variations. Large shields with an angular extent of 20° or more adversely affect the hohlraum efficiency and violate our assumption that the shields do not perturb the hohlraum environment. Because the total P_4 change required is 3%–4%, relatively small shields should suffice. Figure 10 implies that with no other measures, the P_4 asymmetry could be zeroed during the foot pulse with the choice of a 13° shield.

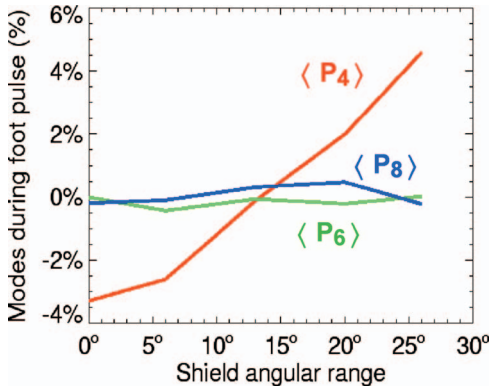

FIG. 10. (Color) P_4-P_8 modes vs shield angular extent for "$P_6=0$" shields.

C. Results with optimized P_4 symmetry shields

LASNEX hohlraum simulations have shown that placing low-density tamping foam in the secondary hohlraum entrance helps maintain an open aperture for radiation flow as well as providing some control of time-dependent P_2 and P_4 asymmetry.[40] In fact, 2D hohlraum simulations with shaped secondary entrance foams alone provide just enough reduction of time-dependent P_2 and P_4 to allow ignition and burn of the capsule, with zero margin. It is important to note that the P_4 shields described above provide an independent P_4 control strategy and can compensate for uncertainties in the calculation of absolute P_4 coefficients. It is clear from Fig. 10 that the initial effect of a shield ring on P_4 is proportional to the shield angular extent. Calculations also show that the time duration over which the shield is affecting P_4 is determined by the radiation burn-through time, which can be controlled via the initial areal density of the shield. Combining the effects of secondary entrance foams and P_4 shields, the best results to date for the baseline capsule and the model pinch power pulse have been obtained using the hohlraum+capsule configuration shown in Fig. 11. The P_4 shield occupies an initial angular range of 4.4° ($\theta_1=50.8°$ and $\theta_2=46.4°$ with respect to the z axis). The shield is 450 μm thick and is composed of 200 mg/cc CH_2 foam with 3 at. %

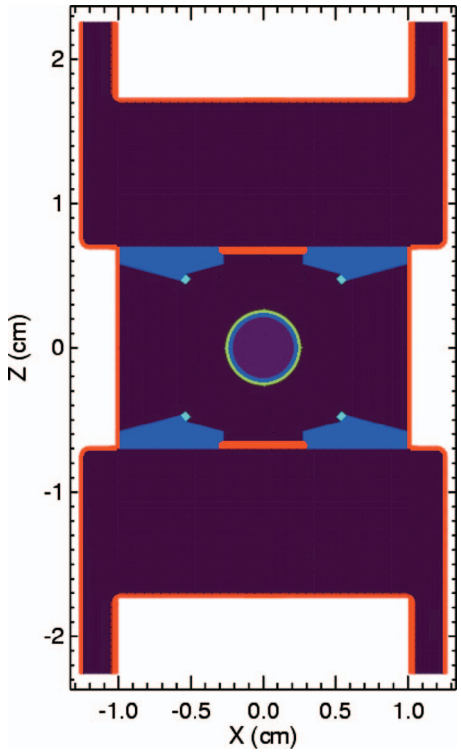

FIG. 11. (Color) Hohlraum configuration with optimum P_4 shields. The secondary entrance tamping foam is 5 mg/cc CH_2 foam and the P_4 shield is 200 mg/cc CH_2 with 3% Ge dopant.

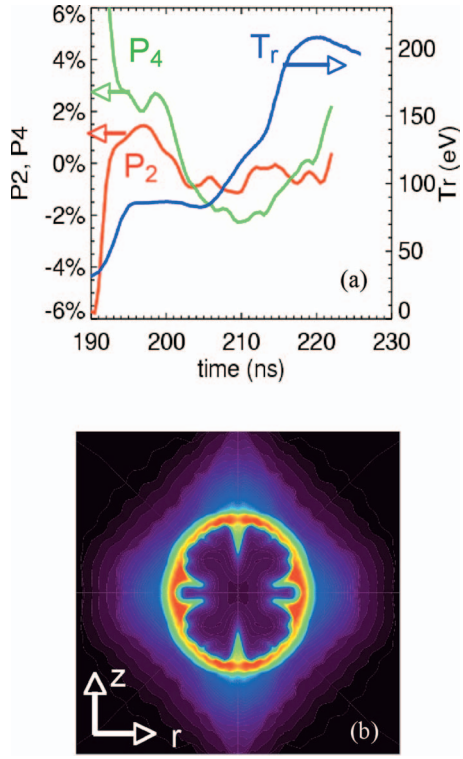

FIG. 12. (Color) (a) Time-dependent P_2 and P_4 in ablation pressure for optimum P_4 shields. (b) DT fuel configuration near ignition time for capsule with 2D yield of 470 MJ.

Ge dopant. A low-density foam annulus tamps the secondary hohlraum entrance, and here this 5 mg/cc CH_2 tamping foam is also used to mount the P_4 symmetry shield ring within the hohlraum. (Alternatively, a few radial spokes could support the P_4 shield, connecting it to the secondary hohlraum wall.) Figure 12(a) shows the resulting time-dependent P_2 and P_4 asymmetry of the capsule ablation pressure, while Fig. 12(b) shows the DT fuel density configuration near ignition time. The 2D yield of this system is 470 MJ, close to the full 1D yield for this capsule. Clearly, the P_4 shield has reversed the sign of the P_4 asymmetry early in the foot, while the swing toward negative P_4 occurs as the radiation burns through the shield, lowering its density and optical depth. In a time-averaged sense, the foot/shoulder values of P_2, P_4, P_6, and P_8 are −0.3%, −0.3%, 0.2%, and 0.1%, respectively. Therefore, this hohlraum design is a significant improvement over the configuration in Fig. 6. Because of the secondary entrance foam, a small 4.4° shield at 200 mg/cc is sufficient to minimize the foot P_4, in contrast to the untamped hohlraum results of Fig. 10 that implied an optimum 13° shield at 100 mg/cc. At the time of peak capsule kinetic energy, the energy absorbed by the P_4 shields is 0.12 MJ compared to the capsule absorbed energy of 1.1 MJ and the total pinch output of 18 MJ, a small energy penalty for providing the very low levels of asymmetry needed for ignition and burn. The tamping foams absorb 0.16 MJ, but the energy investment is well worth it as the foam plasma pressure prevents the expansion of high-Z wall plasma into the secondary entrance, thus improving the transport of radiation from the primary hohlraum to the secondary hohlraum and the capsule. The 2D hohlraum+capsule ignition and burn results are robust to numerical resolution variations. The calculations are also robust to variations in the following:

(a) Shield details: Many examples of shield densities and angular ranges from 2° to 9° have been found to give symmetric implosions and nearly full capsule yield.
(b) Tamping foam details: The density and shape of the secondary entrance foam can be modified to mount various P_4 shields and to control absorption of pre-foot radiation. The foam may also be useful for tamping spoke plasma motion[40] to maintain adequate hohlraum coupling; detailed 3D calculations are planned, but are beyond the scope of the current work.
(c) Magnetic tamping: From solely the hohlraum energetics and symmetry points of view, the primary hohlraum wall motion can be completely untamped and still give capsule ignition and burn.
(d) Z-pinch run-in radiation: Although the hohlraum design can be finely tuned for any level of pre-foot pinch radiation, the results shown are relatively insensitive to assumed run-in levels. A calculation with no run-in radiation at all, with the 4.4° shield and the secondary entrance foam, gave a 2D yield of 390 MJ.

The uniform density, uniform thickness P_4 shield of Fig. 11 is a simple additional structure that enabled symmetric capsule implosion, ignition, and full burn. The time-dependent variation of P_4 shown in Fig. 12(a) could possibly be further reduced by allowing the areal density and/or opac-

ity (e.g., Ge dopant level) of the shield to vary as a function of polar angle. The simple monolithic shield is a technique that can be readily tested in thin-shell capsule backlighting experiments at the Z facility; for example, a series of shields with successively larger angular extent would be expected to result in successively more positive values of P_4 asymmetry at the capsule.

D. Odd mode asymmetry due to top-bottom power imbalance

While hohlraum geometry, additional shields, etc., can control the systematic radiation asymmetry, any hohlraum system driven by energy sources at both ends is in principle susceptible to random top-bottom asymmetries due to power imbalance or mistiming. The most significant effect of such top-bottom imbalances is to introduce odd Legendre mode asymmetry (P_1, P_3, etc.) at the capsule. As shown in Fig. 5, the baseline 520 MJ capsule can tolerate a time-averaged P_1 coefficient of 1.2%, while the 410 MJ capsule tolerates 1.6%. Capsule simulations of the type described in Sec. II B have shown that the 520 MJ capsule can tolerate P_1 asymmetry as high as 8% if the asymmetry occurs only during the foot/shoulder phase, before the capsule has moved very far. Full two-sided 2D LASNEX hohlraum simulations including the optimum P_4 shields were used to relate hypothetical top-bottom source power imbalance or mistiming to P_1 asymmetry at the capsule. These simulations show that for a constant top-bottom power imbalance $\alpha=(P_{\text{bottom}}/P_{\text{top}})-1$ (with perfect timing), the time-averaged foot/shoulder radiation P_1 at the capsule is $\langle P_1\rangle \approx 0.24\alpha$, while for the main pulse $\langle P_1\rangle \approx 0.19\alpha$. These results are valid for α equal to 10% or less.

The shot-to-shot reproducibility experience for wire array Z pinches on Z can be used as some guide to the expected top-bottom pinch similarity for a double-pinch system.[41] Based on 62 hohlraum experiments with 300-wire tungsten wire arrays spanning four years, the standard deviation in peak pinch power as inferred from hohlraum temperature measurements is $\sigma=5.4\%\pm0.5\%$ when the effects of shot-to-shot peak current variations are removed.[18] Stygar *et al.*[41] showed that for two Z pinches sampled from a normal distribution with standard deviation σ, the probability of the power imbalance being less than α is given by $p=\text{erf}(\alpha/2\sigma)$. Combining the hohlraum results relating main pulse P_1 to power imbalance ($P_1=0.19\alpha$) with this probability, one can compute the probability of a double-pinch experiment providing a given level of P_1.[18] These results as applied to this high-yield target are shown in Fig. 13. The curves shown include the nominal case with $\sigma=5.4\%$ and $P_1=0.19\alpha$ (red), an improved Z-pinch reproducibility curve with $\sigma=2.7\%$ and $P_1=0.19\alpha$ (green), and a combination of improved Z-pinch reproducibility and better hohlraum smoothing with $\sigma=2.7\%$ and $P_1=0.14\alpha$ (blue). Table II displays the percentage of shots providing P_1 below the upper limit on capsule tolerance, and the percentage providing P_1 three times lower than the limit. (Although a detailed accounting of potential failure modes for this target has yet to be completed, setting a design specification lower than the upper limit is a step toward providing margin against a combination of potential failure modes.) Improving quality control of Z-pinch load components is a likely path to improved reproducibility that should be explored experimentally, and Fig. 13 and Table II clearly show the effect of a factor of 2 decrease in the shot-to-shot standard deviation. Hohlraum smoothing can also be increased, according to 2D LASNEX simulations, by shaping the secondary hohlraum. An ellipsoidal secondary wall that is 25% larger in radius at the midplane than it is at the secondary entrance provides a P_1 smoothing factor of 0.14 for the main pulse. Increasing both the Z-pinch reproducibility and hohlraum smoothing results in 98% or more of the shots satisfying the upper limits on P_1 for both high-yield capsules.

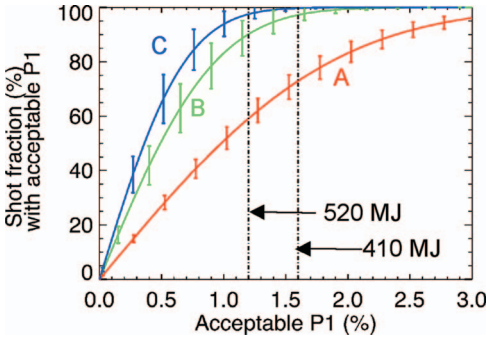

FIG. 13. (Color) Percentage of double-pinch experiments providing a given level of P_1 asymmetry, for: (A) $\sigma=5.4\%$ and $P_1=0.19\alpha$ (nominal reproducibility and hohlraum smoothing), (B) $\sigma=2.7\%$ and $P_1=0.19\alpha$ (increased reproducibility), and (C) $\sigma=2.7\%$ and $P_1=0.14\alpha$ (increased reproducibility and smoothing).

IV. ESTIMATED Z-PINCH LOAD AND ACCELERATOR REQUIREMENTS

In the original scoping study for the double Z-pinch hohlraum concept, a Z-pinch load design based on reduced-density lithium-deuteride (LiD) was proposed.[2] The choice of low atomic number materials was based on calculations showing that radiation trapping (due to material absorption opacity) limits the rate of x-ray power escaping the pinch, for the higher Z-pinch masses required at higher peak currents of 60–70 MA. The present design study seeks to identify a more readily fabricated Z-pinch load that will provide the required total x-ray energy output and the desired pulse

TABLE II. Predicted percentage of shots satisfying P_1 requirements for two high-yield capsule variations.

	520 MJ capsule		410 MJ capsule	
	$P_1<1.2\%$	$P_1<0.4\%$	$P_1<1.6\%$	$P_1<0.53\%$
Nominal reproducibility and hohlraum smoothing $\sigma=5.4\%$ and $P_1=0.19\alpha$	59%	22%	73%	29%
Increased reproducibility $\sigma=2.7\%$ and $P_1=0.19\alpha$	90%	42%	97%	54%
Increased reproducibility and smoothing $\sigma=2.7\%$ and $P_1=0.14\alpha$	98%	55%	>99%	68%

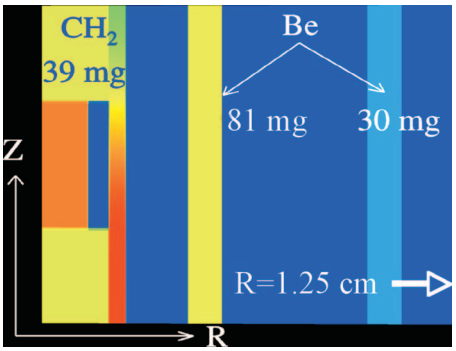

FIG. 14. (Color) Schematic of low-Z multicomponent Z-pinch load being considered for use in the high-yield concept. The precise masses and radii of the various components are design parameters that are varied to tune the timing and level of multiple radiation pulses.

shape. In addition, although it is not clear whether the best Z-pinch performance at higher currents will be provided by wire arrays or by continuous liners, Z-pinch modeling must begin to consider the implications for both options. Although work is still in progress to design a Z-pinch load that satisfies the x-ray output requirements plotted in Fig. 7, a number of physics conclusions can be made here. First, the ongoing simulations confirm the importance of Z-pinch material opacity in trapping x rays and limiting the efficiency with which electrical energy is converted to useful x-ray energy. As a result, present Z-pinch load designs are based on beryllium components. Unlike the LiD used in the initial scoping study, beryllium is readily fabricated in the form of liners or wire arrays, and the conductivity properties of beryllium are expected to allow azimuthally uniform initiation of the current in the load. Quantum molecular dynamics-based wide-range conductivity tables[42] are now available for beryllium, needed to model the range of expected conditions from room temperature solid to high temperature plasma.

One example Z-pinch load configuration being studied is shown in Fig. 14. It includes a Be liner at 1.05 cm radius, an inner Be liner at 0.5 cm radius, and an axially structured on-axis target consisting of Be or CH_2 foam. Typical masses per unit length are 30 mg/cm for the outer liner, 60–80 mg/cm for the inner liner, and 40–50 mg/cm for the on-axis target. The radial positions and masses of these components are chosen to provide the correct timing of the multiple radiation pulses needed to produce the low-adiabat capsule drive of Fig. 3. The collision of the outer and inner Be liners drives a shock through and heats both structures, with the result that the optical depth of the outer liner drops below unity for several nanoseconds, allowing x rays (the foot pulse) to escape radially. The collision of the now-coalesced inner and outer Be liners with the axially structured on-axis target creates a shoulder pulse and the stagnation of the entire mass on axis produces the high power main pulse. Axially varying density in the on-axis target provides 2D shaping of the collision shock that gives the shoulder pulse its desired plateau shape. Axial density gradients in the on-axis target also cause the main stagnation time to vary with axial position ("zippering"), which can be used to give the main pulse its desired height and duration.

It is important to note that the outer Be liner at 30 mg/cm corresponds to a fairly robust 24.6 μm thick liner at solid density (1.85 g/cc). It is thus reasonable to consider nominally 2D axisymmetric initial load configurations such as liners, which may be more readily modeled from room temperature, zero voltage initial conditions than wire arrays, which are inherently 3D from initial conditions onward. However, it is not clear at this point which type of load, wire arrays or liners, will demonstrate more favorable radiation efficiency when scaled up in current. The limited studies of foil-based Z-pinch loads at lower currents have been complicated by poor foil quality and problematic current contact. Nested wire arrays with foam targets have recently demonstrated three-step pulse shapes with the contrast ratios needed for low-adiabat capsule implosions,[43] but their scaling to higher currents must be investigated. Studying and optimizing the x-ray output and pulse shaping from both wire-array and liner-based loads relevant to this high-yield concept should be a focus of near-term pulsed-power experiments.

The circuit model that is presently being used to drive the Z-pinch load design simulations was derived from a preliminary accelerator design based on linear transformer driver (LTD) technology,[44] which is being pursued as a higher efficiency alternative to standard Marx-driven accelerators. This design includes the advanced techniques for electrical power delivery at the petawatt level described in Stygar *et al.*[45] The size of the insulator stack and anode-cathode gaps in the system required to support the high voltages (~30 MV) in a petawatt-class accelerator result in total system inductances of ~30 nH, or about three times higher than the Z facility. A self-consistent accelerator model that is compatible with a 65–70 MA system requires a capacitor stored energy of 340–400 MJ, to drive two pinches with a single radial power feed. This raises the possibility, with a 400 MJ ICF capsule, of setting engineering break-even as a goal for a facility based on this concept. However, considerable research is needed to establish the applicability of LTD technology to ~60 MA, petawatt-class devices. Therefore, a research and development plan is underway to validate an LTD-based accelerator design for future facilities.

V. HIGHER EFFICIENCY AND INTERMEDIATE SCALE OPTIONS

The high-yield target design presented here represents a reference point in hohlraum/capsule design space, for which the energetics and symmetry requirements have been defined. The development of a complete strategy to control radiation symmetry in Legendre modes P_1 through P_8 using a combination of hohlraum geometry, permanent shields, and burn-through shields represents a significant extension of the original hohlraum scoping study, especially given that many of the symmetry control techniques have now been validated experimentally. These techniques represent a general capability for symmetry control in Z-pinch indirect-drive systems. It is now appropriate to consider departures from the reference point presented above, options with higher system efficiency, or intermediate ignition-scale systems that bridge

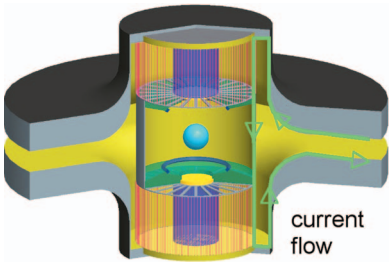

FIG. 15. (Color) Single-feed double Z-pinch geometry in which electrical power is delivered by a midplane disk feed to two Z pinches in series. The secondary entrance foams and P_4 shields are also shown in this figure.

the gap from present-day accelerators to the high-yield concept.

One option under consideration is to drive the two Z pinches in series, as has been done in all double Z-pinch experiments on Z to date.[6,18] In Z experiments, a magnetically-insulated transmission line (MITL) feeding power to the load attaches to the bottom of the Z-pinch load/hohlraum assembly. This means that the primary hohlraum geometry is asymmetric across the midplane (the plane cutting through the center of the capsule), which implies that even with perfectly balanced top-bottom pinch power, the P_1 asymmetry will be nonzero. Alternatively, a single MITL attached as a radial disk feed to the Z-pinch load/hohlraum assembly at the midplane, shown schematically in Fig. 15, restores a top-bottom symmetric hohlraum geometry. A single MITL simplifies the accelerator design. Furthermore, a single MITL feed requires 30% less stored energy to drive the same peak current than an accelerator driving two separate Z pinches via two separate MITLs.[45] LASNEX simulations with the midplane power feed geometry give 2D capsule performance similar to that calculated with the two-sided power feed with the same assumed source x-ray power and current. Low levels of asymmetry and a 2D yield of 460 MJ are obtained for the midplane feed configuration; thus this option has a higher efficiency from the standpoint of capsule absorbed energy (and yield) relative to the stored energy. Questions about the effect of differing radial electric field, above and below the midplane, on the early ablation and implosions of the two Z-pinch loads,[46] must be addressed experimentally and theoretically for this configuration.

The hohlraum energetics relationships for the double Z-pinch hohlraum[2,7] imply that the energy and power necessary to heat the hohlraum to a given temperature scale strongly with the size of the hohlraum. It is also important to note that because the largest sinks of energy are the primary hohlraum walls, and because the x-ray energy enters the secondary hohlraum through an aperture that is essentially the size of the secondary hohlraum, simply decreasing the size of the secondary hohlraum does not increase the drive temperature experienced by the capsule. Dramatic increases in the radiation temperature for a given source power and energy are possible if one can reduce the size of the primary hohlraum. A scaling study using 2D LASNEX quantified the relationship of primary hohlraum temperature to primary hohlraum radius, Z-pinch peak power, and rise time of the power for Gaussian power pulses,[47] and a numerical fit to the results was found. For a fixed pinch power rise time, the peak pinch power required to attain a given peak hohlraum re-emission temperature is given approximately by

$$P \propto (R_p^2 + R_p L_p)^{1.1}, \tag{3}$$

where R_p is the primary hohlraum radius and L_p is the primary hohlraum length. For the nominal hohlraum sizes considered in this paper, with a peak capsule drive temperature of 220 eV, the peak primary hohlraum re-emission temperature is ~240 eV. For example, to attain the same 240 eV peak temperature in a primary with R_p=0.8 cm rather than the nominal 1.25 cm, expression (3) implies that the Z-pinch power and energy could be scaled down by a factor of 0.48. This option must be more precisely defined in simulations but would represent a significant increase in system efficiency as defined by the ratio of the capsule absorbed energy to the stored energy. While hohlraum size strongly influences the energetics requirements, incremental increases in hohlraum efficiency can be realized with further optimization of mixed-component hohlraum walls,[48] slightly shorter Z-pinch loads and primary hohlraums, optimizing the spoke transmission, or allowing some radiation burn-through of the on-axis shine shields.[47]

The hohlraum size energetics scaling can be extended to other temperatures assuming $P \sim T_r^{3.3}$,[7] seeking intermediate-scale, higher temperature hohlraum systems that achieve ignition at the ~50 MJ level. For example, a Scale 0.6 hohlraum intended to drive a 1.6 mm radius capsule with a shorter pulse peaking at 250 eV, with a primary hohlraum radius of 0.75 cm and length of 0.6 cm and an initial Z-pinch load radius of 0.6 cm, is estimated to require a peak primary hohlraum temperature of 270 eV and therefore a peak pinch power of 465 TW per side using expression (3). (Using the more general energetics scaling that includes the effect of the shorter rise time for the more compact system, the result is 525 TW per side.) LASNEX hohlraum simulations of such a system (including the secondary entrance foams and P_4 shields discussed in Sec. III C) demonstrate that a shaped temperature pulse peaking at 250 eV can indeed be achieved with a peak power of 550 TW per pinch and a total useful x-ray energy of 3.0 MJ per pinch, delivering ~0.4 MJ to the capsule. Such a temperature pulse is compatible with higher implosion velocity, lower yield capsules. A number of ideas for generating high x-ray power from compact sources have been proposed and tested on 1 MA class machines, and their performance must be tested at the 20 MA level and above. These include planar wire arrays,[49] radial wire arrays,[50] X pinches,[49] and short implosion time compact single[51] and nested wire arrays[52] (the latter two having undergone preliminary tests at 20 MA on Z). As x-ray sources and primary hohlraums can be made more compact, secondary entrance tamping, hohlraum wall tamping, and mode-selective symmetry control techniques will become even more important to provide adequate energy coupling and symmetry control.

VI. CONCLUSIONS

The initial scoping study of the double Z-pinch hohlraum inertial fusion concept has been revisited with particular attention to capsule robustness, hohlraum symmetry control, and Z-pinch pulse shaping. Capsules with 1D yields of 400–500 MJ are insensitive to relatively large variations in the three-step temperature pulse timing and level, show tolerance of surface roughness at levels well above that achievable with today's fabrication technology, and tolerate radiation asymmetry levels that are attainable with hohlraum symmetry control techniques. Fine tuning of the time-dependent radiation symmetry has been demonstrated for the first time in simulations using small-angular-range shields that specifically tune the P_4 asymmetry without perturbing the P_6, P_8, or higher modes. Maintaining low levels of asymmetry has enabled the demonstration of robust ignition and burn of the capsule in 2D integrated hohlraum+capsule simulations yielding 470 MJ. The capsule and hohlraum energetics results determine the goal of the Z-pinch load design research, which is ongoing: the generation of a 9 MJ x-ray pulse properly shaped with a 0.5 MJ foot pulse generated 15–20 ns prior to peak power. Several Z-pinch load variations are currently being pursued in simulations to generate the required pulse. Looking ahead, improvements in the overall system efficiency look promising using variations on the reference design such as a midplane feed-driven system to improve the accelerator/Z-pinch efficiency, as well as compact x-ray sources and compact primary hohlraums which may allow ignition-class experiments to be conducted with stored energies higher than present accelerators but lower than the high-yield concept.

ACKNOWLEDGMENTS

We would like to thank Dr. Debra Callahan, Dr. Jim Hammer, Dr. Judy Harte, Dr. John Lindl, Dr. Steve MacLaren, and Dr. George Zimmerman (LLNL) for valuable discussions on the LASNEX simulations, as well as Mark Johnston (Ktech, SNL) and Lee Busby (LLNL) for LASNEX computing support. We also acknowledge the enthusiastic programmatic support of Dr. Keith Matzen.

Sandia is a multiprogram laboratory operated by Sandia Corporation, a Lockheed Martin Company, for the United States Department of Energy's National Nuclear Security Administration under Contract No. DE-AC04-94AL85000.

[1] T. W. L. Sanford, G. O. Allshouse, B. M. Marder *et al.*, Phys. Rev. Lett. **77**, 5063 (1996); C. Deeney, T. J. Nash, R. B. Spielman *et al.*, Phys. Rev. E **56**, 5945 (1997).
[2] J. H. Hammer, M. Tabak, S. C. Wilks, J. D. Lindl, D. S. Bailey, P. W. Rambo, A. Toor, G. B. Zimmerman, and J. L. Porter, Jr., Phys. Plasmas **6**, 2129 (1999).
[3] R. B. Spielman, C. Deeney, G. A. Chandler *et al.*, Phys. Plasmas **5**, 2105 (1998).
[4] J. L. Porter, Jr., Bull. Am. Phys. Soc. **42**, 1948 (1997); K. L. Baker, J. L. Porter, L. E. Ruggles *et al.*, Appl. Phys. Lett. **75**, 775 (1999).
[5] M. E. Cuneo, R. A. Vesey, J. L. Porter, Jr. *et al.*, Bull. Am. Phys. Soc. **44**, 40 (1999).
[6] M. E. Cuneo, R. A. Vesey, J. L. Porter, Jr. *et al.*, Phys. Plasmas **8**, 2257 (2001).
[7] M. E. Cuneo, R. A. Vesey, J. H. Hammer, J. L. Porter, Jr., L. E. Ruggles, and W. W. Simpson, Laser Part. Beams **19**, 481 (2001).
[8] R. A. Vesey and T. A. Mehlhorn, Bull. Am. Phys. Soc. **43**, 1903 (1998); R. A. Vesey, M. Cuneo, D. Hanson, J. Porter, T. Mehlhorn, L. Ruggles, W. Simpson, M. Vargas, J. Hammer, and O. Landen, *ibid.* **44**, 227 (1999); R. A. Vesey, M. E. Cuneo, D. L. Hanson, J. L. Porter, Jr., T. A. Mehlhorn, L. E. Ruggles, W. W. Simpson, J. H. Hammer, and O. Landen, *ibid.* **45**, 360 (2000).
[9] R. A. Vesey, D. L. Hanson, M. E. Cuneo, G. R. Bennett, J. L. Porter, T. A. Mehlhorn, J. H. Hammer, R. G. Adams, L. E. Ruggles, and W. W. Simpson, in *Inertial Fusion Sciences and Applications 2001*, edited by K. A. Tanaka, D. D. Meyerhofer, and J. Meyer-ter-Vehn (Elsevier, Paris, 2002), p. 681.
[10] M. E. Cuneo, R. A. Vesey, J. L. Porter, Jr. *et al.*, Phys. Rev. Lett. **88**, 215004 (2002).
[11] G. R. Bennett, O. L. Landen, R. F. Adams, J. L. Porter, L. E. Ruggles, W. W. Simpson, and C. Wakefield, Rev. Sci. Instrum. **72**, 657 (2001).
[12] G. R. Bennett, M. E. Cuneo, R. A. Vesey *et al.*, Phys. Rev. Lett. **89**, 245002 (2002).
[13] D. B. Sinars, M. E. Cuneo, G. R. Bennett *et al.*, Rev. Sci. Instrum. **74**, 2202 (2003).
[14] R. A. Vesey, M. E. Cuneo, G. R. Bennett *et al.*, Phys. Rev. Lett. **90**, 035005 (2003).
[15] R. A. Vesey, M. E. Cuneo, J. L. Porter, Jr. *et al.*, Phys. Plasmas **10**, 1854 (2003).
[16] R. A. Vesey, M. E. Cuneo, G. R. Bennett, J. L. Porter, and T. A. Mehlhorn, Bull. Am. Phys. Soc. **50**, 123 (2005).
[17] R. A. Vesey, M. E. Cuneo, G. R. Bennett, J. L. Porter, and T. A. Mehlhorn, J. Phys. IV **133**, 1167 (2006).
[18] M. E. Cuneo, R. A. Vesey, G. R. Bennett *et al.*, Plasma Phys. Controlled Fusion **48**, R1 (2006).
[19] G. B. Zimmerman and W. L. Kruer, Comments Plasma Phys. Controlled Fusion **2**, 51 (1975).
[20] S. W. Haan (personal communication).
[21] M. C. Herrmann, M. Tabak, and J. D. Lindl, Nucl. Fusion **41**, 99 (2001); D. H. Munro, P. M. Celliers, G. W. Collins, D. M. Gold, L. B. DaSilva, S. W. Haan, R. C. Cauble, B. A. Hammel, and W. W. Hsing, Phys. Plasmas **8**, 2245 (2001).
[22] W. J. Krauser, N. M. Hoffman, D. C. Wilson *et al.*, Phys. Plasmas **3**, 2084 (1996).
[23] T. R. Dittrich, S. W. Haan, M. M. Marinak, S. M. Pollaine, and R. McEachern, Phys. Plasmas **5**, 3708 (1998).
[24] M. M. Marinak, G. D. Kerbel, N. A. Gentile, O. Jones, D. Munro, S. Pollaine, T. R. Dittrich, and S. W. Haan, Phys. Plasmas **8**, 2275 (2001).
[25] T. R. Dittrich, S. W. Haan, M. M. Marinak *et al.*, Phys. Plasmas **6**, 2164 (1999).
[26] R. M. More, K. H. Warren, D. A. Young, and G. B. Zimmerman, Phys. Fluids **31**, 3059 (1988).
[27] See National Technical Information Service Document DE-96004569 (M. M. Marinak, R. E. Tipton, B. A. Remington, S. W. Haan, and S. V. Weber, in ICF Quarterly Report, UCRL-LR-105821-95-3, 1995). Copies may be ordered from National Technical Information Service, Springfield, VA 22161.
[28] The NIF standard spectrum mode coefficients in nm are expressed as $R_{lm}=10/l^{1.5}+0.08/[(l/60)^{0.7}+(l/1200)^4]$ for the mode range typically used in multimode calculations. As used in the 2D axisymmetric simulations, each l mode contains the perturbation power of the $(21+l)$ azimuthal m modes.
[29] S. W. Haan, M. C. Herrmann, T. R. Dittrich, A. J. Fetterman, M. M. Marinak, D. H. Munro, S. M. Pollaine, J. D. Salmonson, G. L. Strobel, and L. J. Suter, Phys. Plasmas **12**, 056316 (2005).
[30] A. Nikroo, K. C. Chen, M. L. Hoppe *et al.*, Phys. Plasmas **13**, 056302 (2006).
[31] S. Pollaine, P. Amendt, S. Haan, M. Herrmann, O. Jones, and L. Suter, in *Inertial Fusion Sciences and Applications 2003*, edited by B. A. Hammel, D. D. Meyerhofer, J. Meyer-ter-Vehn, and H. Azechi (ANS, La Grange Park, IL, 2004), p. 104.
[32] T. J. Orzechowski, M. D. Rosen, H. N. Kornblum, J. L. Porter, L. J. Suter, A. R. Thiessen, and R. J. Wallace, Phys. Rev. Lett. **77**, 3545 (1996).
[33] S. W. Haan, S. M. Pollaine, J. D. Lindl *et al.*, Phys. Plasmas **2**, 2480 (1995); M. Tabak and D. Callahan-Miller, *ibid.* **5**, 1895 (1998).
[34] M. E. Cuneo, E. M. Waisman, S. V. Lebedev *et al.*, Phys. Rev. E **71**, 046406 (2005).
[35] A. Caruso and C. Strangio, Jpn. J. Appl. Phys., Part 1 **30**, 1095 (1991).

[36]M. E. Cuneo, G. R. Bennett, R. A. Vesey *et al.*, Bull. Am. Phys. Soc. **48**, 207 (2003).
[37]G. R. Bennett, M. E. Cuneo, R. A. Vesey *et al.*, Bull. Am. Phys. Soc. **48**, 207 (2003).
[38]See National Technical Information Services Document No. DE95011970 (T. J. Murphy and P. A. Amendt, ICF Quarterly Report Vol. 4, pp. 101, 1994, Lawrence Livermore National Laboratory, UCRL-LR-105821-94-3), copies may be ordered from National Technical Information Service, Springfield, VA 22161; D. D.-M. Ho, J. A. Harte, and M. Tabak, Nucl. Fusion **35**, 1125 (1995); D. L. Hanson, R. A. Vesey, M. E. Cuneo *et al.*, Phys. Plasmas **9**, 2173 (2002).
[39]D. A. Callahan, M. C. Herrmann, and M. Tabak, Laser Part. Beams **20**, 405 (2002); D. A. Callahan, M. Tabak, G. R. Bennett, M. E. Cuneo, R. A. Vesey, A. Nikroo, D. Czechowicz, and D. Steinman, Plasma Phys. Controlled Fusion **47**, B379 (2005).
[40]Spoke array simulations more recent than those mentioned in Refs. 2 and 6 indicate that low-density foam in the secondary entrance also tamps the expansion and axial flow of ablated spoke plasma, leading to possibly more ideal spoke behavior. There is also experimental experience with secondary tamping foams. Recent Z experiments on hohlraum coupling and capsule symmetry, which have been used to validate 2D hohlraum simulations, included a combination of radial spoke arrays and low-density foams at the secondary entrance. X-ray transmission values of $67\pm5\%$ were measured for this configuration (Ref. 18), consistent with the $71\pm7\%$ inferred for cases without foam.
[41]W. A. Stygar, H. C. Ives, D. L. Fehl *et al.*, Phys. Rev. E **69**, 046403 (2004).
[42]M. P. Desjarlais, J. D. Kress, and L. A. Collins, Phys. Rev. E **66**, 025401 (2002).
[43]M. E. Cuneo, R. A. Vesey, D. B. Sinars *et al.*, Phys. Rev. Lett. **95**, 185001 (2005).
[44]M. G. Mazarakis, R. B. Spielman, K. W. Struve, and F. W. Long, in *Proceedings of the 13th IEEE International Pulse Power Conference*, edited by R. Reinovsky and M. Newtonon (IEEE, Piscataway, NJ, 2001), p. 587; M. G. Mazarakis, W. E. Fowler, F. W. Long, D. H. McDaniel, C. L. Olson, S. T. Rogowski, R. A. Sharpe, and K. W. Struve, in *Proceedings of the 15th IEEE International Pulse Power Conference* (IEEE, Piscataway, NJ, 2005).
[45]W. A. Stygar, M. E. Cuneo, R. A. Vesey *et al.*, Phys. Rev. E **72**, 026404 (2005); W. A. Stygar, M. E. Cuneo, D. I. Headley, H. C. Ives, R. J. Leeper, M. G. Mazarakis, C. L. Olson, J. L. Porter, and T. C. Wagoner, "Architecture of petawatt-class Z-pinch accelerators," Phys. Rev. ST Accel. Beams (to be published).
[46]S. N. Bland, S. V. Lebedev, J. P. Chittenden *et al.*, Phys. Rev. Lett. **95**, 135001 (2005).
[47]R. A. Vesey, M. E. Cuneo, G. R. Bennett, J. L. Porter, and T. A. Mehlhorn, Bull. Am. Phys. Soc. **49**, 279 (2004).
[48]L. J. Suter, J. Rothenburg, D. Munro, B. Van Wonterghem, and S. Haan, Phys. Plasmas **7**, 2092 (2000).
[49]V. L. Kantsyrev, A. S. Safronova, D. A. Fedin *et al.*, IEEE Trans. Plasma Sci. **34**, 194 (2006).
[50]S. V. Lebedev, A. Ciardi, D. J. Ampleford *et al.*, Plasma Phys. Controlled Fusion **47**, B465 (2005); S. N. Bland, Bull. Am. Phys. Soc. **51**, 338 (2006).
[51]D. B. Sinars (personal communication).
[52]M. E. Cuneo, D. B. Sinars, E. M. Waisman *et al.*, Phys. Plasmas **13**, 056318 (2006).